Inter-hemispheric Decadal Variations in SST, Surface Wind, Heat Flux and Cloud Cover over the Atlantic Ocean

Youichi TANIMOTO

Graduate School of Environmental Earth Science, Hokkaido University, Sapporo, Japan
Frontier Research System for Global Change, Yokohama, Japan

and

Shang-Ping XIE

International Pacific Research Center and Department of Meteorology, University of Hawaii, HI, USA

(Manuscript received 9 October 2001, in revised form 27 June 2002)

Abstract

Atlantic decadal climate variations are studied using marine meteorological observations. To remove artificial interhemispheric correlation, we perform empirical orthogonal function (EOF) analysis of sea surface temperature (SST) variability separately for the North and South Atlantic. The first EOF for the North (South) Atlantic in the decadal (8–16 years) band features a meridional tripole (dipole). In the tropics, the northern and southern leading EOFs form a meridional dipole with a center of action at 15° on either side of the equator. The leading sea level pressure (SLP) EOFs for the North and South Atlantic each feature a center of action that is displaced poleward of the tropical SST extreme, at 30° latitude. The SLP center of action in the North Atlantic has a barotropic structure and contributes significantly to surface wind variability in the tropics. Despite being derived from statistically independent data samples, the principle components for the leading SST and SLP EOFs (four in total) are significantly correlated with one another, indicative of the existence of an interhemispheric mode spanning the entire Atlantic Ocean. The same analysis for a longer SST record suggests that this pan-Atlantic decadal variability exists throughout the 20th century.

In the North Atlantic, composite analysis of wind velocity and heat fluxes based on the PCs of the leading SST modes indicates that wind-induced latent heat flux is the major forcing for decadal SST variability. In the South Atlantic, by contrast, wind anomalies are neither organized in space nor in geostrophic balance with SLP, a problem likely due to poor sampling there as indicated by a comparison with well-sampled satellite measurements.

Spatially coherent anomalies of low-level cloud cover are found to be associated with the tropical Atlantic dipole, with increased (decreased) cloudiness over the cold (warm) lobe. These low-level cloud anomalies do not appear to be associated with significant surface wind convergence, unlike the deep convective clouds near the equator. By shielding solar radiation, these low-level cloud anomalies act to reinforce the underlying SST anomalies, reducing the Newtonian cooling rate for SST by as much as 30%.

1. Introduction

Tropical Atlantic sea surface temperatures (SSTs) affect the rainfall variability on surrounding continents including northeastern Brazil, Sahel and western equatorial Africa

Corresponding author: Youichi Tanimoto, Graduate School of Environmental Earth Science, Hokkaido University, Sapporo 060-0810, Japan.
E-mail: tanimoto@ees.hokudai.ac.jp

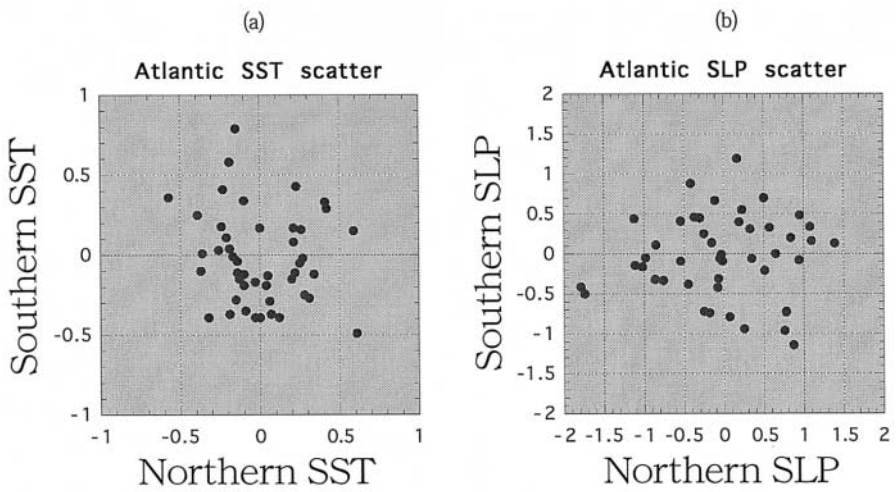

Fig. 1. Scatter plots of zonal-mean (a) SST (°C) and (b) SLP (hPa) anomalies in the northern and southern tropics. Zonal mean anomalies are calculated from coast to coast using unfiltered boreal-winter data in the 8–20° latitude for SST and 20–40° for SLP.

(Hastenrath and Heller 1977; Lamb 1978). Recent empirical and modeling studies further suggest that boreal winter SST anomalies in the tropical Atlantic may excite teleconnection into the extratropics, affecting eastern North America and Europe (Rajagopalan et al. 1998; Watanabe and Kimoto 1999; Robertson et al. 2000; Okumura et al. 2001).

There is a general consensus that SST anomalies (SSTAs) in the equatorial Atlantic are involved in a zonal interaction with the atmosphere (Zebiak 1993; Huang et al. 1995; Ruiz-Barradas et al. 2000), much akin to El Niño/Southern Oscillation (ENSO) in the equatorial Pacific. Unlike the Pacific, however, SST variance does not have a local maximum on the equator in the Atlantic; the variance is comparable or even larger in the subtropical (10–30°) than equatorial Atlantic. The cause of this subtropical SST variability in the Atlantic is not well understood.

Previous attempts to empirically determine the modes of tropical Atlantic SST variability have yielded mixed and sometimes mutually conflicting results. Empirical orthogonal function (EOF) analysis suggests a monopole with the same sign over the tropical Atlantic and a meridional dipole of opposing signs across the ITCZ (e.g., Servain 1991), with the two explaining similar amounts of variance. Joint EOF and/or Singular Value Decomposition (SVD) methods pick the dipole as the leading mode, along with a well-known connection to the meridional shift of the Atlantic ITCZ and anomalous precipitation in northeastern Brazil (Nobre and Shukla 1996; Chang et al. 1997). In an attempt to relax the orthogonal requirement of the normal EOF analysis, Houghton and Tourre (1992) rotate the EOFs to maximize regional variance and show that a pair of leading rotated EOFs share similar amount variance, each with high loading confined to one side of the equator and little signal on the other side. This, plus the fact that SSTAs are not linearly correlated across the equator (Fig. 1), leads them to suggest that SST variability in the northern and southern tropical Atlantic is physically independent, a conclusion supported by Mehta's (1998) analysis using a combination of statistical methods. When decadal time scales are separated from the interannual variability in the modal decomposition analyses, the northern and southern tropical SSTAs in boreal winter-spring are negatively correlated on the decadal time scale, while those are positively correlated on the interannual time scales (Enfield et al. 1999, Tanimoto and Xie 1999).

Tropical Atlantic SST does not vary in isolation but rather in association with the extratropical Atlantic. The tropical North Atlantic SSTAs are correlated with those in the extratropical North Atlantic, forming the so-called wintertime tripole pattern (Deser and Blackmon 1993; Kushnir 1994; Halliwell and Mayer

1996; Lau and Nath 2001). Similarly, SSTAs in the tropical and extratropical South Atlantic are correlated (Venegas et al. 1997). On decadal time scales, observational studies suggest that SST variability may be correlated over the whole Atlantic basin from the South Atlantic to Greenland (Xie and Tanimoto 1998; Rajagopalan et al. 1998; Tourre et al. 1999; Tanimoto and Xie 1999). During boreal winter-spring seasons, as part of this so-called pan-Atlantic decadal oscillation (PADO), the tropical dipole, with a strong cross-equatorial SST gradient that forces the ITCZ to move in the meridional direction, is apparently involved in a two-way tropical-extratropical interaction with the NAO (North Atlantic Oscillation) as model studies suggest (Xie and Tanimoto 1998; Okumura et al. 2001; Sutton et al. 2001). When a northward cross-equatorial SST gradient occurs, sea level pressure (SLP) anomaly field shows a southward gradient, whose centers of action are displaced poleward of maximum tropical SSTAs and found at 30° (Tanimoto and Xie 1999). Some atmospheric general circulation models (GCMs) reproduce this SLP signal as a wintertime response to a tropical SST dipole (Okumura et al. 2001; Sutton et al. 2001; N.-C. Lau, personal comm.), while some show no response in any season (Dommenget and Latif 2000; Chang et al. 2000). The physical mechanisms for tropical and extratropical interaction in the Atlantic remain to be further studied.

The present study revisits the issue of interhemispheric structure of decadal variability in the Atlantic by taking a different approach than previous studies. Most previous studies applied modal decomposition analyses to a domain that includes both the northern and southern tropical Atlantic, and then examined spatial loadings. This may force an artificial correlation across the equator as Houghton and Tourre (1992) illustrated. To avoid this possibility of artificial interhemispheric correlation, we carry out EOF analysis separately for the North and South Atlantic. Recognizing tropical-extratropical interaction, we will include extratropical Atlantic in our analysis domains. Thus, we do not assume a priori that there is an interhemispheric mode but instead check posteriorly whether such an interhemispheric correlation exists by correlating the leading principal components for the North and South Atlantic and comparing their spatial patterns. We will further repeat the same analysis for the SLP field and examine if the leading EOFs are correlated between the North and South Atlantic and with the SST EOFs. This will give information as to the interaction of the ocean and atmosphere.

On interannual to decadal time scales, surface heat flux forcing by the atmosphere is the major mechanism for SST variability in off-equatorial oceans (Alexander 1992; Cayan 1992; Wagner 1996; Lau and Nath 1996, 2001; Carton et al. 1996). In the tropics, an ocean-atmospheric feedback mechanism involving surface wind, evaporation and SST (WES; Xie and Philander 1994) favors a mode of equatorially anti-symmetric structure that seems to correspond to the SST dipole in the tropical Atlantic (Chang et al. 1997; Xie et al. 1999). Lagged crosscorrelation between meridional wind anomalies and SST gradient near the equator presents a symmetric distribution of correlation as a function of lead-lag months, which indicates two-way air-sea interaction at least in the equatorial region (Chang et al. 2001). In addition to wind-induced evaporation, the atmosphere can change SSTs through cloud-induced radiation anomalies (Klein and Hartmann 1993; Philander et al. 1996; Park and Leovy 2000). Recently, Okumura et al. (2001) report a positive feedback between SST and low-level clouds in the tropical Atlantic in analyzing observational and GCM data. In this paper, we will examine the latent, sensible and radiative heat flux associated with the leading SST EOFs in the Atlantic basin and investigate whether these flux anomalies can explain the SST anomalies fully or something else such as ocean dynamics may also play a role.

Two types of gridded SST datasets are available. One type uses optimal interpolation to fill data at every grid point in order to provide boundary conditions for atmospheric GCMs. The global sea ice and SST (GISST; Parker et al. 1994) dataset belongs to this category. The other gridding method fills a grid point only when there are enough number of observations; the comprehensive ocean-atmosphere dataset (COADS) is such an example. Many empirical studies (Mehta 1998; Enfield et al. 1999; Xie et al. 1999) have employed the former

dataset to capture basin-scale structure of Atlantic SST anomalies. Over data sparse region like the South Atlantic, however, heavy temporal and spatial interpolations can be a source of signal distortion. Here we construct a dataset using the ship-board measurements alone and require all grid points in the analysis to have uninterrupted seasonal means (see the next section for details) to ensure the fidelity of the gridded data and check the results using the GISST data.

The rest of the paper is organized as follows; Section 2 describes the datasets and the analysis procedures. Section 3 shows the leading EOF modes that happen to explain the meridional gradients of the inter-tropical SST and SLP anomaly fields. Section 4 presents the pan-Atlantic patterns for SST, SLP, wind velocity and surface turbulence heat fluxes. Section 5 describes the associated cloud anomaly pattern and its feedback on SST. Section 6 discusses the possible mechanisms for the pan-Atlantic variability and Section 7 is a summary.

2. Data and analysis procedure

A monthly 4° latitude-longitude dataset of marine meteorological variables is constructed from quality-controlled ship and buoy observations compiled in Long Marine Reports in fixed length records (LMRF) of comprehensive ocean-atmosphere dataset (COADS; Woodruff et al. 1987) for the North and South Atlantic (70°N–40°S) from 1950 through 1995. The domain contains the Norwegian, North and Caribbean Seas, the southern part of the Labrador Sea, Gulf of Mexico and Mediterranean. In the present study, we examine SST, SLP, vector and scalar wind speed, sensible and latent heat flux fields. Higher resolution ($2^\circ \times 2^\circ$) dataset of total and low-level cloudiness is also constructed from ship reports in COADS LMRF that are based on visual estimate of cloud coverage. Turbulence heat fluxes are calculated using Kondo's (1975) aerodynamic bulk method for each ship-buoy measurement and averaged into the monthly dataset. The solar radiation and net longwave radiation are estimated by the formula of Reed (1977) and Clark et al. (1974), respectively. Details of calculation procedure are described in Tanimoto et al. (1997) and Iwasaka and Hanawa (1990).

In constructing this dataset, we do not use satellite-based observations to avoid possible systematic bias due to instrument changes. No spatial interpolation is made so this new dataset serves as a strong check against optimally interpolated datasets like GISST. Because of a possible systematic bias of SST data around the 1940s due to changes in the number of observations and instrumental technique (Deser and Blackmon 1993; Folland and Parker 1995), we will only use the COADS for a 46-year period after 1950.

We will use the GISST (1900–1997) to infer the modal structure in earlier decades that are not well covered by COADS. We will further employ historical surface temperature dataset based on only instrumental observations (Parker et al. 1995; Jones et al. 2001) to validate the results from GISST. In regions like the South Atlantic where there are few ship observations, COADS suffers severe sampling errors; SLP and wind velocity may not even satisfy the geostrophic balance. To complement results based on the COADS, we use the monthly 2° latitude-longitude National Centers for Environmental Prediction (NCEP) reanalysis dataset (Kalnay et al. 1996) for 1958–1995 that provides dynamically consistent SLP and wind velocity data. At each grid point, we calculate the monthly climatological mean annual cycle based on the entire period of record (COADS: 46 years; NCEP: 38 years; GISST: 98 years), and the monthly anomalies are defined as the departures from the climatological means.

The NAO and associated SST tripole pattern are very pronounced in boreal winter but is not seen in summer (Deser and Blackmon 1993; Kushnir 1994). To ensure characteristics of the PADO, we further construct averages for boreal winters (December through March) and require more than three monthly-mean values each winter to fill a grid point. Our EOF analysis of COADS SST and SLP anomalies is carried out only at those grid points that contain no missing boreal-winter averages for the entire period of 1950/51 through 1994/95. There are 312 (103) such grid points for the North (South) Atlantic SST field, and 314 (113) for the North (South) Atlantic SLP. Uninterrupted data record for 46 years may be too strong a requirement more than enough to ensure a meaningful EOF analysis, but we intentionally

set this rather stringent criterion for data inclusion to contrast with the GISST analysis.

Large variance is found in the tropical SST anomaly field on interannual and decadal time scales (Servain 1991; Huang and Shukla 1997; Mehta 1998) with a spectral gap between the two time scales (Mehta and Delworth 1995; Mehta 1998; Enfield et al. 1999). A closer look of the spectral structure for pan-Atlantic SST variability by Tourre et al. (1999) also presents interannual (2.7-, 3.5-, and 4.4-year) and quasi-decadal (11.4-year) time scales of which spatial structures represent different coherent patterns to each other. Significant spectral peaks above the red noise are also identified at decadal time scales in other variables such as northwest Brazil rainfall (Mehta 1998), and 835-year high-resolution sediment core in the southern Caribbean Sea (Black et al. 1999). Based on the above spectral structure of tropical Atlantic SST anomalies, Tanimoto and Xie (1999) applied a time-scale separation method to the 51-year SST time series and found negative (positive) correlation on decadal (interannual) time scale in SST anomalies across the equator. Here we use a four-pole Butterworth recursive band-pass filter similar to Tanimoto and Xie's to extract decadal variations. Cut-off periods of the band-pass filter are eight and sixteen years, respectively. The decadal SST (SLP) variance represents 14% (11%) of the unfiltered winter variance over the whole Atlantic basin.

3. Inter-hemispheric structure

Before performing the EOF analysis, we divide the Atlantic basin into two parts north and south of the equator to eliminate possible artificial correlation between them that may arise from EOF decomposition as discussed in Section 1. Our analysis domains include both the tropical and extratropical Atlantic: 0–70°N and 0–40°S (0–50°S) for COADS (GISST). Then, SST anomalies are averaged for boreal winter and filtered through a decadal band of 8–16 year, a frequency domain that contains large SST variance (Servain 1991; Mehta 1998; Rajagopalan et al. 1998; Tourre et al. 1999).

3.1 COADS (1950–95)

The upper two curves in Fig. 2 show normalized principle components (PCs) of the first SST modes in the North (solid) and South (dashed) Atlantic, respectively, based on COADS. Figure 3 depicts the SST regressions onto these PCs. Grid points used in the EOF analysis are shaded in the background. The loadings of these leading EOFs explain 35.0% and 28.9% (4.8% and 4.0%) of the band-passed (unfiltered) variance at all the grid points over the entire Atlantic basin, both north and south (Table 1). The percentages to the total decadal

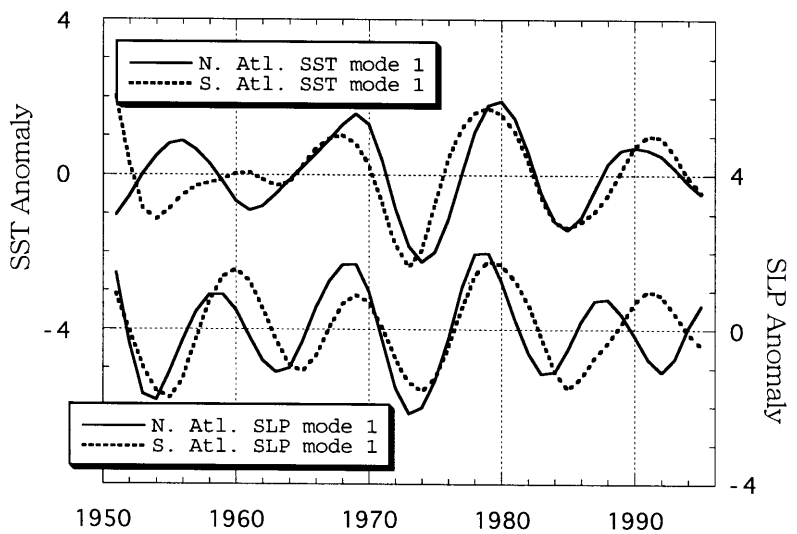

Fig. 2. Upper curves: normalized principal components (PCs) of SST anomalies in the North (solid) and South (dashed line) Atlantic. Lower: PCs of SLP anomalies.

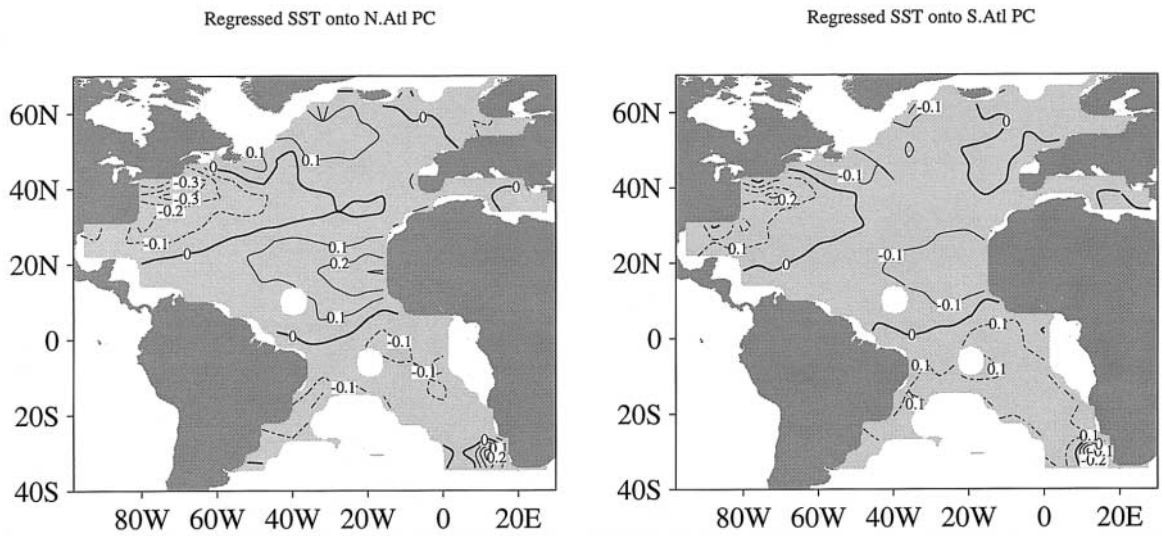

Fig. 3. The first SST EOFs for the North and the South Atlantic, which explain 35.0% and 28.9% (4.8% and 4.0%) of decadal band-passed (unfiltered) boreal-winter SST anomalies over their respective domains. Grid points used in the EOF analysis are shaded. SST regression onto the North (South) Atlantic PC is shown in the left (right) panel. Contour interval is 0.1°C, with negative values dashed.

Table 1. Explained percentage of leading EOFs to the total unfiltered (left column) and decadal (right column) variances of particular domains. Upper (lower) two matrices are for a domain of North (South) Atlantic.

1st. EOF for	SST-North Atlantic		SLP-North Atlantic	
Domain	Unfiltered	Decadal	Unfiltered	Decadal
Pan Atlantic	4.8	35.0	4.0	35.9
North Atlantic	5.5	37.0	4.0	36.5

1st. EOF for	SST-South Atlantic		SLP-South Atlantic	
Domain	Unfiltered	Decadal	Unfiltered	Decadal
Pan Atlantic	4.0	28.9	2.0	18.0
South Atlantic	6.2	54.9	6.0	50.2

and unfiltered variances of a particular subdomain are also listed in Table 1. The first modes accounts for 37.0% and 54.9% of the decadal variance in the North and South Atlantic, respectively, and are well separated from the second modes, which explain only 19.0% and 13.2% of the decadal variance, respectively. The leading EOF for the North Atlantic features the tripole mode (Deser and Blackmon 1993; Kushnir 1994) with positive centers of action in the tropics and high latitudes (55°N) and a negative center in between in the midlatitudes (40°N). The South Atlantic EOF shows a rather uniform negative loading except in the southeastern corner where the poor data coverage gives rise to a spurious center of action. The spatial structure of SST anomalies will be further discussed in Section 4.

We note that these leading EOFs are derived from statistically independent subsets of the COADS so there is no *a priori* reason for them to be correlated. Yet the PCs of these separate EOFs are positively correlated (Fig. 2), with a simultaneous correlation coefficient of 0.63. In the tropics, their centers of action have opposing signs across the equator (Fig. 3). The regression patterns in Fig. 3 are very similar to the PADO of Xie and Tanimoto (1998). Simultaneous correlation maps with the two PCs show similar spatial pattern to the regression maps (not shown), with the correlation coefficients exceeding 0.8 at all the centers of action.

We repeat the same analysis for the boreal-winter SLP fields in the two sub-domains (Fig. 4). The loadings in leading SLP modes explain 35.9% and 18.0% (4.0% and 2.0%) of band-passed (unfiltered) variance in the Pan-Atlantic basin. A negative SLP center of action appears in the 20–40°N band in the subtropical North

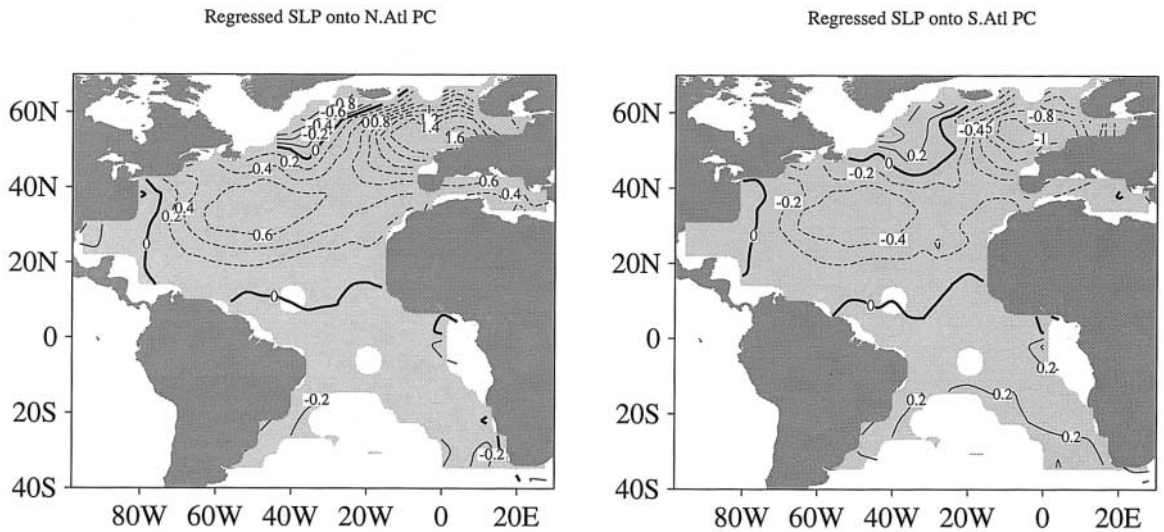

Fig. 4. Same as Fig. 3, but for SLP. These EOFs explain 35.9% and 18.0% (4.0% and 2.0%) of decadal band-passed (unfiltered) boreal winter SLP anomalies for the North and the South Atlantic, respectively. Contour interval is 0.2 hPa.

Table 2. Correlation between the leading PCs of SST and SLP variability in the North and South Atlantic.

Index	SLP North Atlantic	SLP South Atlantic	SST North Atlantic	SST South Atlantic
SLP North Atlantic	1	0.63	0.56	0.69
SLP South Atlantic	*	1	0.5	0.78
SST North Atlantic	*	*	1	0.63

Atlantic, which is 10–15° poleward of the positive SST center in the tropics. The extratropical center west of Europe also has significant regressions. The South Atlantic loadings do not have much spatial structure, but with a slight southward gradient SLP. The accompanying PCs of the SLP EOFs for the North (solid) and South (dashed line of Fig. 2) Atlantic correlate to one another. Furthermore, the SST and SLP pairs of PCs are correlated among themselves despite that they are derived from independent samples (Table 2). In particular, two minima in the early 1970s and 1980s and three maxima in the late 1960s, late 1970s and early 1990s appear in all four time series (Fig. 2). These results indicate that a PADO involving SST and SLP is quite pronounced for the recent three decades. Scatter plots of zonal mean values in the 20–40°N and 20–40°S bands, calculated from band-pass filtered SLP anomalies (not shown), confirm an out-of-phase relationship with a tilted elliptical track much like the scatters of decadal SST anomalies (see Fig. 5 in Tanimoto and Xie 1999).

We also perform an SVD analysis for the SST and SLP fields over the combined North and South Atlantic. The leading SVD mode explains 60.1% of total squared covariance. The heterogeneous regression maps of SST and SLP fields (not shown) are similar to the regression fields in Figs. 3 and 4. This is consistent with Tourre et al. (1999). This PADO pattern with zonal bands of SSTAs with alternating signs is simulated in ocean models forced by observed wind variability (Seager et al. 2000) and in a coupled GCM (Watabane et al. 1999).

3.2 GISST (1901–97)

The correlation among four PCs in Fig. 2 is highest for the three decades from 1966 through 1990. (If performed for a shorted period of 1966–1995, the EOFs for SST and SLP explain about 15% more decadal variance in each sub-domain.) Before 1966 and after 1990, however, their correlation is not as good. Since this could be due to the end effect of the band-pass filter, we use the longer GISST dataset and perform the same EOF analysis for three periods: the entire 20th century (1901–

Table 3. Explained percentage of leading EOFs to the total unfiltered (left column) and decadal (right column) variances of particular domains. Upper (lower) three matrices are for a domain of North (South) Atlantic. The left (middle, right) matrices represent percentages during the period of 1901–97 (1950–97, 1901–49).

1st. EOF for	GISST North Atlantic(1901-97)		GISST North Atlantic(1950-97)		GISST North Atlantic(1901-49)	
Domain	Unfiltered	Decadal	Unfiltered	Decadal	Unfiltered	Decadal
Pan Atlantic	2.9	27.4	5.0	34.9	2.3	26.8
North Atlantic	4.5	35.6	6.9	44.2	2.8	28.0

1st. EOF for	GISST South Atlantic(1901-97)		GISST South Atlantic(1950-97)		GISST South Atlantic(1901-49)	
Domain	Unfiltered	Decadal	Unfiltered	Decadal	Unfiltered	Decadal
Pan Atlantic	2.7	25.2	4.7	32.8	2.9	33.2
South Atlantic	3.5	39.7	6.4	49.7	3.8	50.7

1997) and its first (1901–1949) and second (1950–1997) halves. The percentages to the total decadal and unfiltered variances of a particular sub-domain over each period are also listed in Table 3. It is not surprising that the leading EOFs for 1950–1997 (not shown) is nearly the same as those in Fig. 3. Most updated PCs for the entire Atlantic are available at the author's web site (see appendix).

The North Atlantic EOF for 97 years of the 20th century (Fig. 5a) is also similar to that for the recent four decades except for a more zonally uniform structure in the tropics. The South Atlantic EOF for 1901–1997 appears quite different from that for 1950–1997 with a dipole

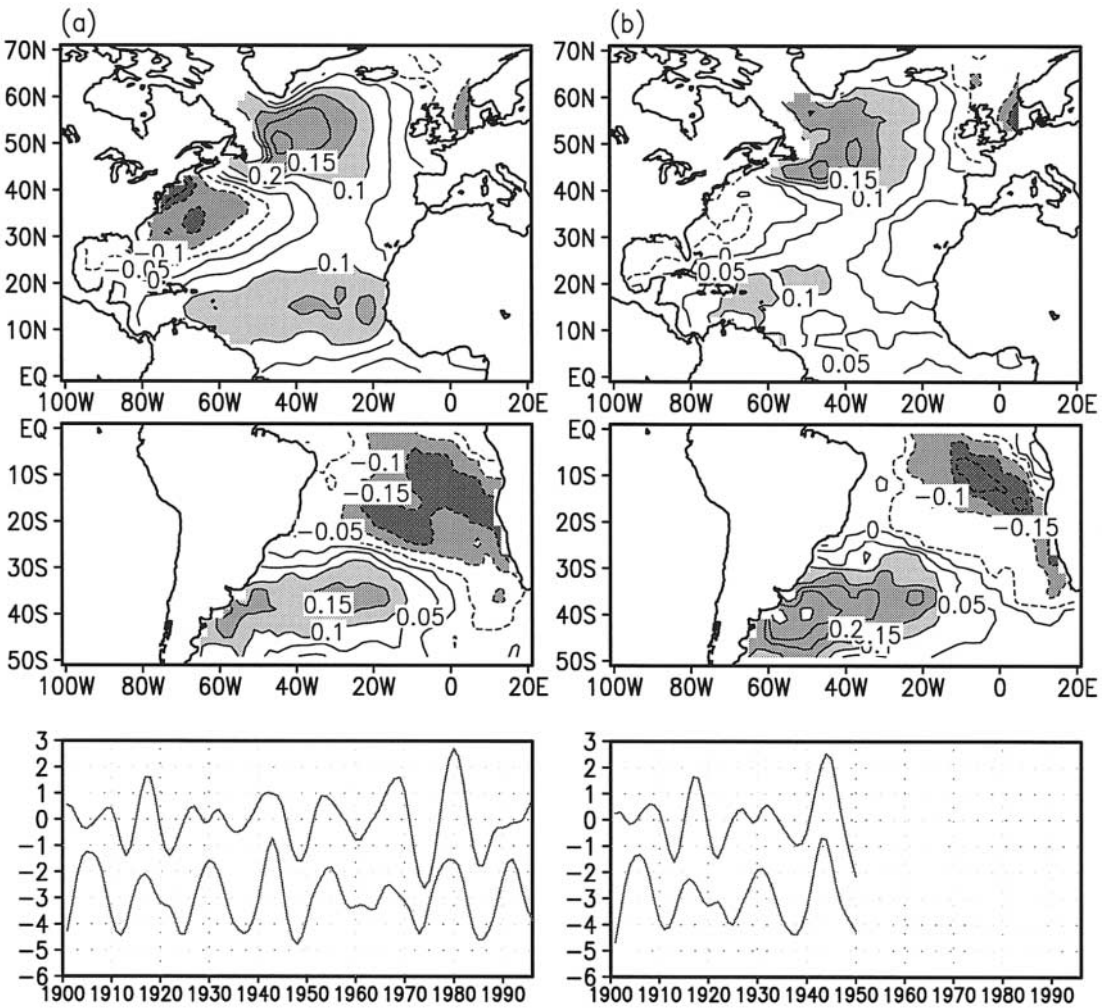

Fig. 5. Same as Fig. 3, but for GISST during (a) 1901–97 and (b) 1901–1949. Contour interval is 0.05°C, with negative values dashed. Table 3 displays the variance explained by these EOFs. The upper (lower) curve in the bottom panel shows the North (South) Atlantic PC.

Table 4. Correlation between the leading PCs of SST variability in the North and South Atlantic for three different periods.

Index	SST North Atlantic (1901-97)	SST South Atlantic (1901-97)	SST North Atlantic (1901-49)	SST South Atlantic (1901-49)
SST North Atlantic (1901-97)	1	0.57	0.79	0.39
SST South Atlantic (1901-97)	*	1	0.58	0.92
SST North Atlantic (1901-49)	*	*	1	0.66

structure between the tropics and midlatitudes as opposed to a uniform field in Fig. 3. A close look suggests that these differences arise rather from the lack of midlatitude South Atlantic information in the COADS analysis due to our stringent requirement of having undisrupted coverage at every grid point. This South Atlantic dipole has been discussed by Venegas et al. (1997). The North and South Atlantic PCs are again positively correlated (Table 4).

The right panels of Fig. 5 are the EOFs for the first half of the 20th century, which resemble those to the left with some differences in details. We note that the North Atlantic tripole now becomes the second mode explaining 28.2% of the total variance. The first North Atlantic mode for this period explains slightly more variance (29.7%, not shown) but high loadings are confined only along the east coast of North America. Hence trivial degeneracy and mixing of eigenvalues may not occur among these two modes. The North Atlantic tripole is still highly correlated with the South Atlantic dipole for this earlier period (corr = 0.57; Table 4). The correlation between the North and South Atlantic PCs improves significantly for 1950–66. Thus the apparent variable correlation in our COADS analysis is indeed due to the end effect of our band-pass filter.

One may cast doubt on the usefulness of our EOF analysis for the earlier period on the grounds that the optimal interpolation scheme for GISST uses the EOFs for the later period to fill data voids. To address this concern, we carry out a composite analysis by choosing twelve (eleven) years when the PCs for 1901–1949 are in the positive (1901–02, 1909–10, 1926–27, 1940–45) and negative (1912–13, 1921–24, 1935–36, 1947–49) phase. (The World War I period has not been included.) Figure 6 shows the difference between those positive and negative phase years, based on the instrumental observations both on the land and over the ocean (Parker et al. 1995; Jones et al. 2001). The difference map is quite similar to the EOFs derived from the heavily spatial-interpolated GISST. Land temperature anomalies over northern South America, eastern North America and Europe are quite well organized and have the same sign as those in the neighboring seas.

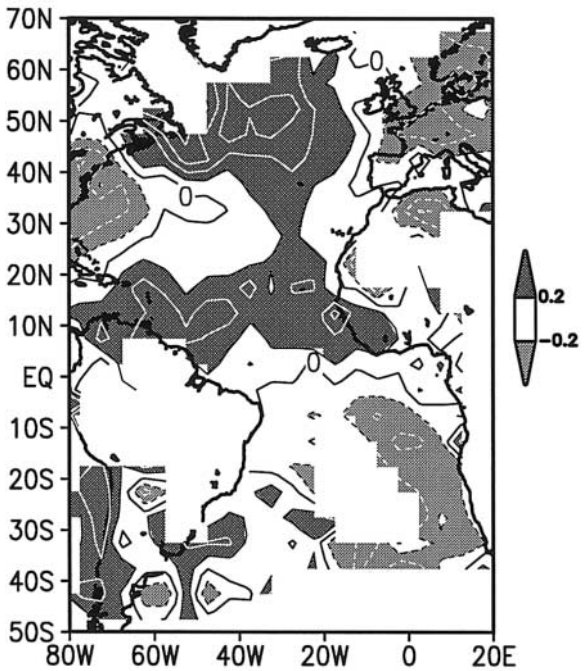

Fig. 6. Difference of unfiltered boreal-winter surface temperature between the positive and negative phases of the PCs for 1901–49. Contour intervals are 0.2°C, with negative values dashed.

4. Pan-Atlantic decadal variability

The above analyses of different datasets using the EOF and composite techniques suggest that Atlantic decadal variability has a high degree of interhemispheric coherence at decadal timescales and that this PADO mode is quite robust during most of the 20th century. In this section, we focus on the three recent cycles of the PADO, taking advantage of more abundant observations. Six years each are chosen to

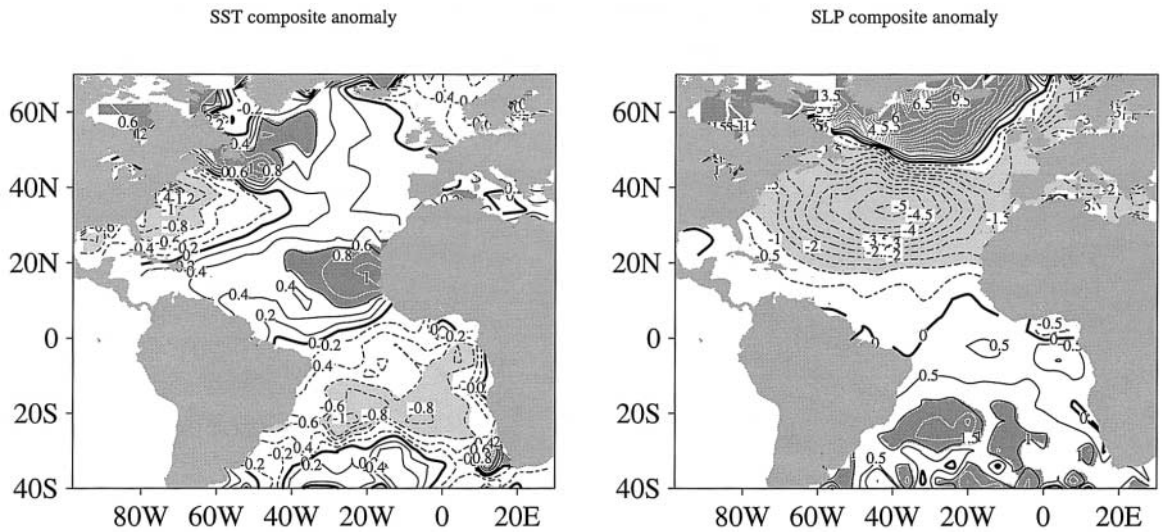

Fig. 7. Difference of unfiltered boreal-winter SST and SLP between six positive (1968, 69, 70, 79, 80, 81) and six negative (1972, 73, 74, 84, 85, 86) PADO-phase years. Contour interval is 0.2°C and 0.5 hPa for SST and SLP fields, respectively. Negative values are dashed.

represent PADO's positive (1968–1970, 1979–1981) and negative (1972–1974, 1984–1986) phases. The positive phase here refers to a northward SST gradient in the tropics. We will show difference maps between the two phases based on the COADS without any spatial interpolation/smoothing.

4.1 North Atlantic

The difference map for SST (Fig. 7) in the Northern Hemisphere is similar to the EOFs in Figs. 3 and 5. The amplitudes are comparable between the northern and southern tropics, with maximum values at about 1°C. The positive pole in the midlatitude South Atlantic appears in this composite map much like that in the EOF based on GISST. The SLP pattern (Fig. 7) in the North Atlantic is similar to the EOF in Fig. 4 except for a reduced signal west of Europe. Though noisy over the South Atlantic, the SLP difference map indicates a consistent southward gradient up to 20°S in the tropics.

Anomalous wind velocity in the North Atlantic is well organized in space and apparently in geostrophic balance with SLP anomalies (Fig. 8a). The anomalous easterlies north of 35°N reduce the local wind speed in the mid- and high latitudes. South of the center of anomalously low SLP, the anomalous westerlies reduce (increase) the speed of the prevailing trade (westerly) winds south (north) of 30°N. The maximum reduction in trade wind speed reaches 1.5 ms^{-1} (light shade in Fig. 8), suppressing local latent heat flux release from the ocean surface (Fig. 9). The anomalous circulation at the surface induces large anomalies in latent heat flux that act to cause local SST anomalies (Alexander 1992; Cayan 1992; Lau and Nath 2001). In the high-latitude North Atlantic, the anomalous sensible heat flux (Fig. 9) is comparable with the latent one. A recent atmospheric GCM study shows that the anomalous surface circulation in the tropical and midlatitude North Atlantic, including the reduced trade winds and enhanced cold surge on the east coast of North America, is a response to tropical SST-induced changes in deep convection (Okumura et al. 2001).

The cross-equatorial southerlies are a robust feature near the equator, in response to a northward SST gradient anomaly. Anomalous winds converge (diverge) just north (south) of the equator, causing an anomalous northward shift of the ITCZ (Fig. 10b) and droughts in northeastern Brazil.

4.2 South Atlantic

South of 10°S, anomalous wind vectors are not well organized, and neither are the latent and sensible heat flux anomalies. The South Atlantic (10–40°S) is very poorly observed; the

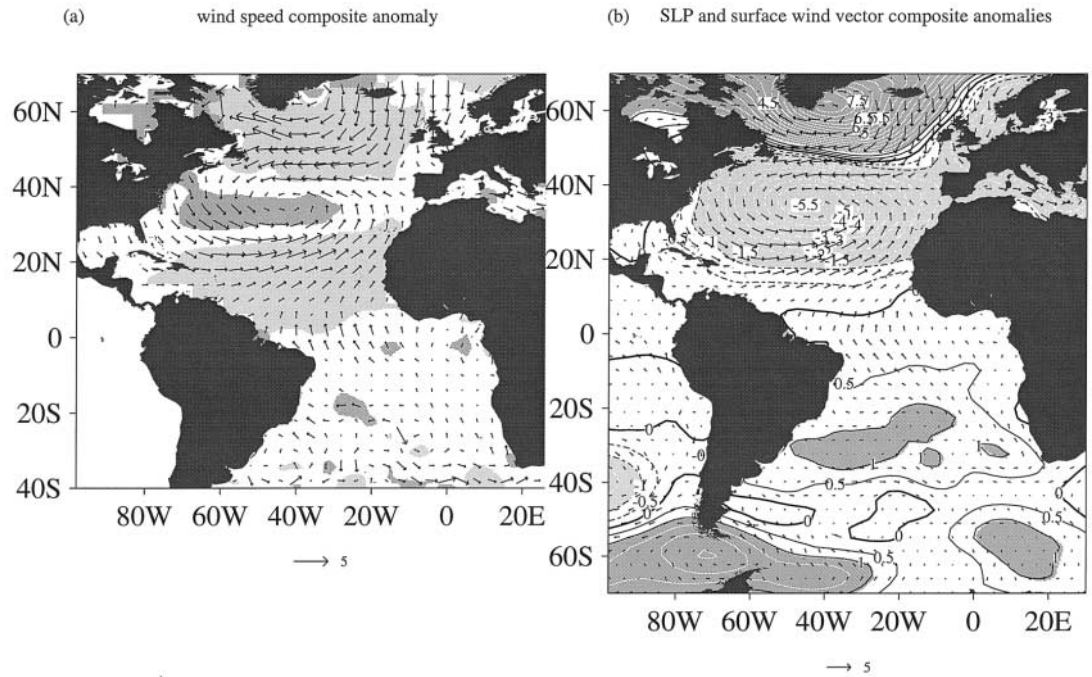

Fig. 8. (a) Same as Fig. 7, but for wind velocity anomalies (vectors with the scale in 5 ms^{-1} displayed at the bottom). Dark (light) shades denote scalar wind speed anomalies that exceed 0.5 (-0.5) ms^{-1}. (b) Same as Fig. 8a, but for SLP and wind velocity from the NCEP reanalysis. Contour interval is 0.5 hPa for the SLP field, with negative values dashed.

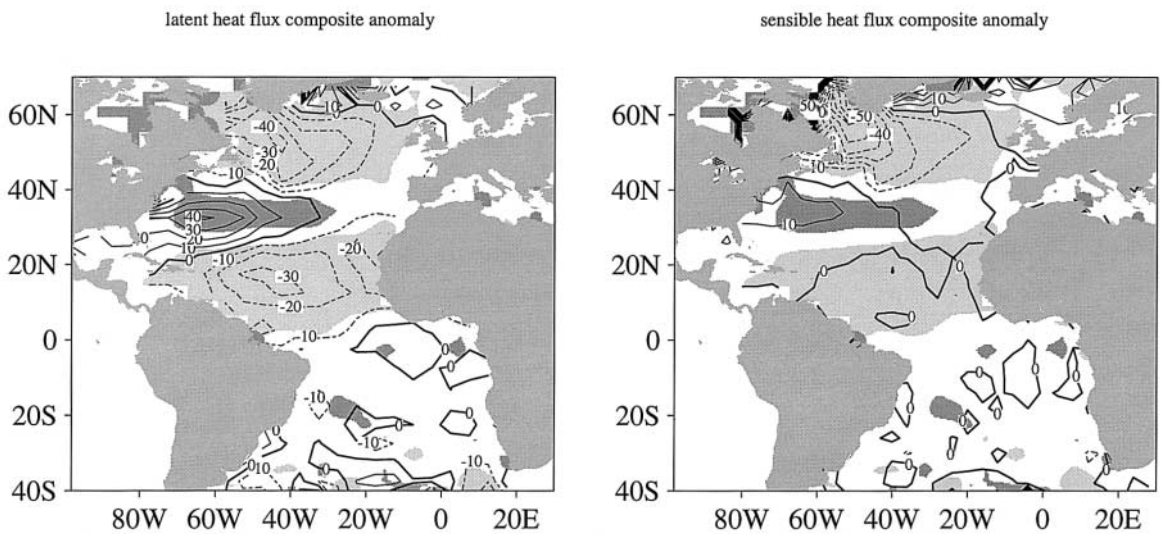

Fig. 9. Same as Fig. 7 but for latent and sensible heat flux anomalies (upward positive). Contour interval is 10 Wm^{-2}. Same shades in Fig. 8a are superimposed.

total number of simultaneous observations of SST, air temperature, relative humidity and wind velocity registered in COADS is 5.1×10^5 as opposed to 2.4×10^6 for the North Atlantic (10–40°N) for the period of 1961–1990. Over much of the South Atlantic, anomalous winds are not in geostrophic balance with the SLP even in a qualitative sense. Previous modal de-

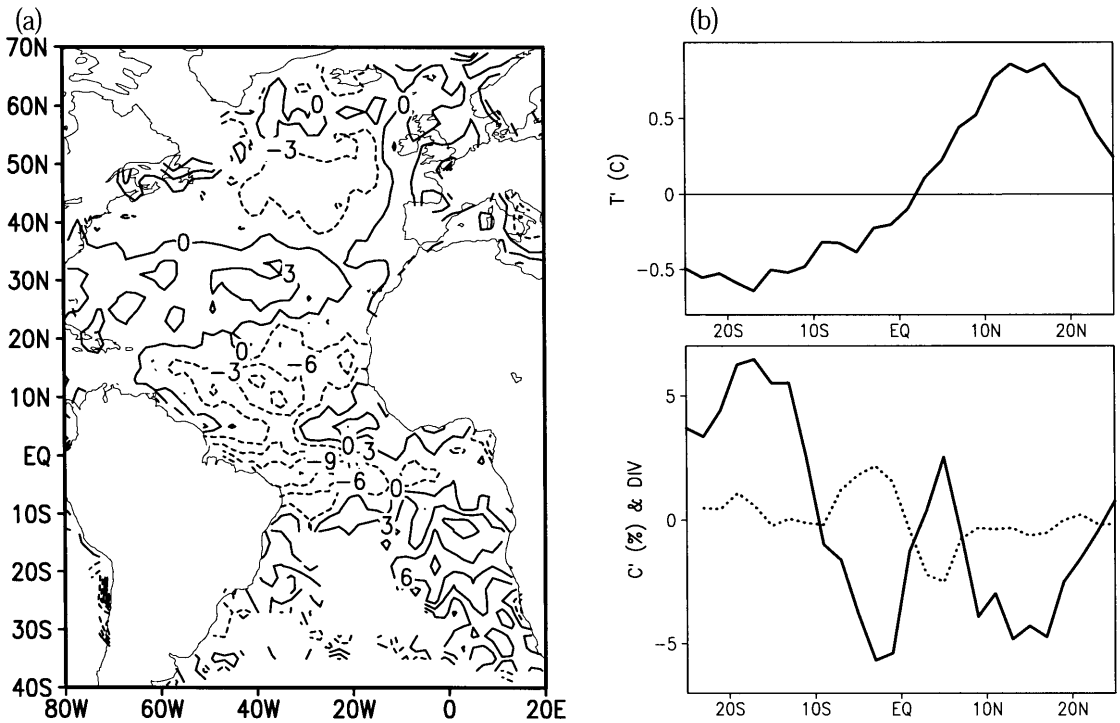

Fig. 10. (a) Difference of unfiltered February–April total cloud cover anomalies (contours at intervals of 3.0%) between positive and negative phases of the PADO, based on a $2^\circ \times 2^\circ$ COADS. (b) Zonal mean anomalies of SST (upper right) and cloud cover (%; solid) along with surface wind divergence (10^{-6} s^{-1} in dotted line; lower right panel).

composition analyses (Enfield and Mayer 1997; Mestas-Nuñez and Enfield 1999) also yield a strong SLP signal but no associated wind signal in the South Atlantic.

We repeat the composite analysis using the NCEP reanalysis. In the North Atlantic, both the resultant wind velocity and SLP maps (Fig. 8b) closely resemble those based on COADS. In the South Atlantic, by contrast, anomalous winds become much better organized, in geostrophic wind balance (down the SLP gradient) off (near) the equator. A positive SLP center is found around 30°S, slightly poleward of the negative SST center in the tropical South Atlantic. The southeasterly trades intensify north of this SLP center, implying an evaporative cooling that is consistent with the observed SST anomalies underneath. South of this SLP center along 40°S, the NCEP reanalysis shows enhanced westerlies that would act to cool the SST instead of a warming in the COADS composite. This inconsistency between observed SSTAs and local winds in the extratropical South Atlantic can be due to the poor sampling/reanalysis errors or an indication that ocean processes other than surface heat flux and Ekman advection may be at work there (Häkkinen and Mo 2002). We note that the Brazil current leaves the coast and joins the Antarctic Circumpolar Current around 40°S, along which the southern lobe of the South Atlantic dipole is located. Ocean dynamics is important for SST variability in such western boundary current extension regions (e.g., Tomita et al. 2002).

Among the three variables we analyze here, SST varies on the slowest time scales (>1 month) and is least subject to sampling errors. SLP has large spatial scales (>1000 km) and is less susceptible to turbulence fluctuations than wind velocity, which is related to the spatial derivative of SLP. It is quite clear that traditional ship-board wind measurements are not enough to sample the South Atlantic properly. The NCEP dynamic assimilation system significantly improves the wind product by including SLP measurements. Still, the inconsistency

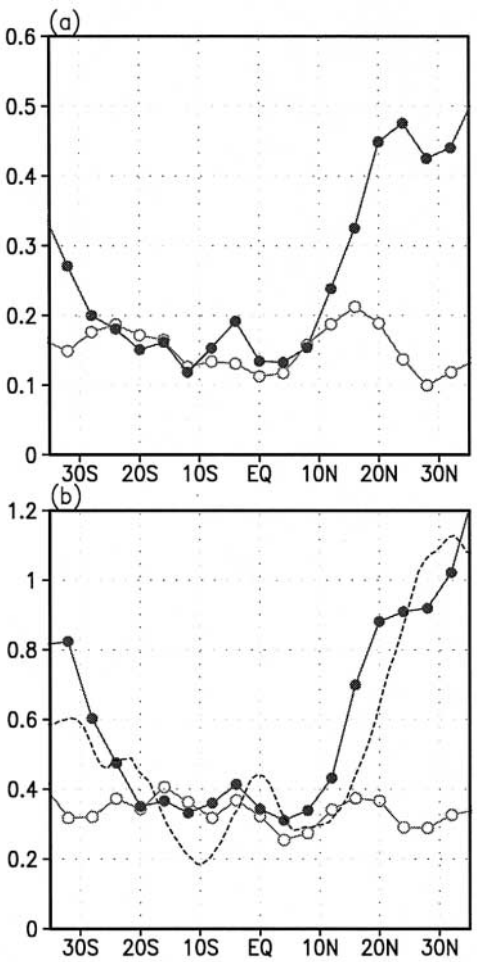

Fig. 11. (a) Zonal-mean standard deviations of zonal wind velocity (thick line with closed circles) and SST (light line with open circles) in the decadal band. (b) Same as Fig. 11a, but for the unfiltered total variance for eight years from COADS (line with filled circles) and ERS satellites (dashed). The climatological mean is computed from the eight-year data used.

in the input data between wind velocity and SLP is likely to have introduced errors in the wind analysis and obscured the wind signals on climatic time scales.

Satellite scatterometers offer a great potential of improving wind measurements over traditionally poorly observed oceans such as the South Atlantic (e.g., Hashizume et al. 2001). Figure 11 compares standard deviations of boreal-winter zonal wind velocity observed by European Remote Sensing (ERS) satellites for 1992–2000 and that based on COADS for 1987–1995. ERS scatterometers measure wind velocity averaged over a $0.5^\circ \times 0.5^\circ$ grid box and at a weekly resolution. Even over well ship-sampled North Atlantic, COADS wind variance tends to be larger than the ERS. Much of the variance difference in the North Atlantic may be due to difference in sampling. COADS samples wind velocity at a single point and thus contains high-frequency, small-scale fluctuations while ERS scatterometers measure large-scale wind velocity averaged over a $0.5^\circ \times 0.5^\circ$ area.

To demonstrate the effectiveness of space wind observations, Fig. 12 compares 1994–1993 wind velocity differences based on COADS and ERS, along with COADS SLP differences. In the North Atlantic, COADS samples the wind field quite well, which is apparently in geostrophic balance with concurrently measured SLP anomalies. The 1994–93 difference fields feature a strong anomalous low (high) in the high- (mid-) latitude North Atlantic. In particular, the mid-latitude high has two centers at 70°W and 20°W, respectively, which are both associated with enclosed anticyclonic flow. Thus, in the North Atlantic, the ERS wind anomalies are similar to the well-sampled COADS fields, both qualitatively and quantitatively.

By design, the ERS scatterometers sample the South Atlantic winds at the same frequency as in the North Atlantic. The 1994–93 wind differences are weakly easterly (<3 m/s) in the tropical South Atlantic, with a maximum at 0°E, 12°S, and feature weakened westerlies in 30–40°S. The COADS wind differences are generally noisy and not well organized in space (the southerlies off northeastern Brazil are the exception). The fact that the ERS wind anomalies are not in geostrophic balance with COADS SLP anomalies in the South Atlantic suggests that the latter also suffers from severe sampling errors, at least on interannual timescales.

5. Cloud feedbacks

In boreal winter-spring seasons when the SST field in the equatorial Atlantic is nearly uniform in both the zonal and meridional directions, the ITCZ is sensitive to the changes in interhemispheric SST gradient (Nobre and

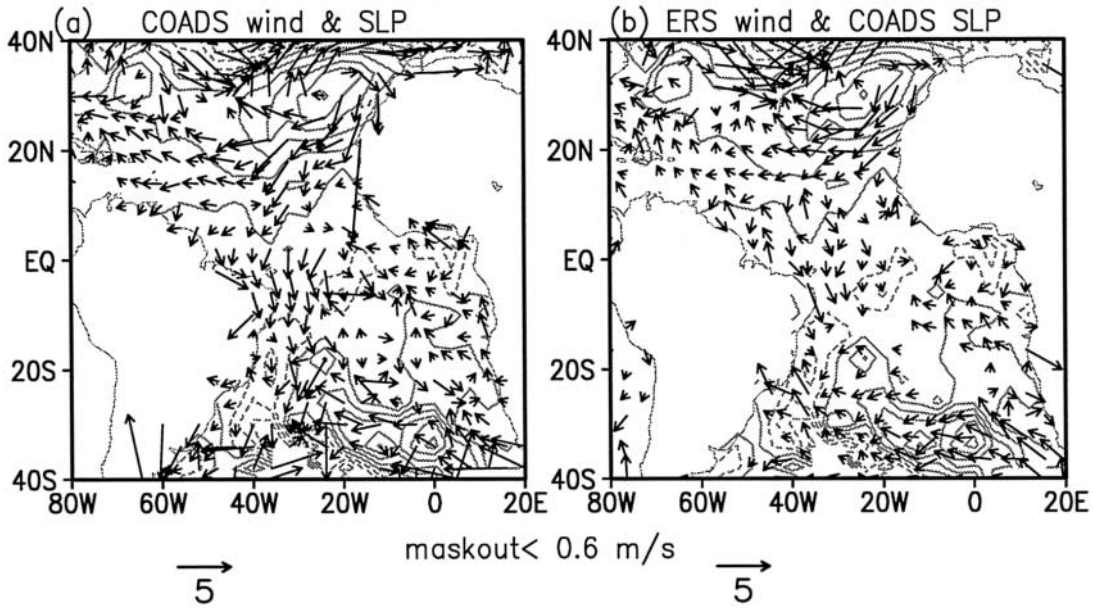

Fig. 12. (a) February–March difference of COADS SLP and wind velocity between 1994 and 1993. Contour interval is 1 hPa. The wind velocity scale (ms^{-1}) is placed at the bottom. (b) Same as Fig. 12a, but for wind velocity difference based on ERS scatterometers.

Shukla 1996). The associated meridional shifts of the ITCZ cause northeastern Brazil rainfall to fluctuate, leading to droughts or floods (Servain 1991; Mehta 1998; Chiang et al. 2000). Figure 10a shows a difference map of cloudiness anomalies between positive and negative phases based on a 2° resolution COADS. Associated with an anomalous northward gradient of zonal mean SST anomalies is an increase (decrease) in cloudiness at 5°N (5°S; Fig. 10b), indicating a northward shift in ITCZ's latitude. These near-equatorial changes in cloudiness seem associated with enhanced (suppressed) convective activity over positive (negative) SST anomalies as indicated by the convergence (divergence) of anomalous winds at the surface (dotted line in Fig. 10b). Thus, in the near-equatorial region, more high clouds form over warm SST anomalies, reducing incoming solar radiation and underlying SST anomalies. This near-equatorial damping may not have much effect on the meridional SST gradient over the whole tropics because SST anomaly extremes are located near 15–20°N/S.

Additional cloudiness anomalies are found over SST anomaly extremes poleward of 10° latitude on both sides of the equator. These off-equatorial cloudiness anomalies, in contrast, are negatively correlated with local SST anomaly, but apparently not associated with significant changes in surface wind convergence. More than 90% of the anomalies in these subtropical regions are due to changes in low-level clouds (Fig. 13a) such as stratus and stratocumulus. Over a positive SST anomaly, the boundary layer warming may reduce the static stability at its top, a condition disfavoring the stratus formation (Klein and Hartmann 1993). Even without any spatial smoothing in our dataset, these low-level cloud anomalies are quite well organized in latitudinal bands between 10 and 20° (Fig. 10). The total radiative flux is about 10 Wm^{-2} cooling (heating) over positive (negative) cloudiness anomalies, with shortwave dominating longwave forcing (Fig. 13b). The radiative forcing by low-level clouds is a positive feedback on SST[1]. Such opposite response of the equatorial and subtropical

1 After the submission of this paper, an independent but complementary study came to our attention. By cross-correlating observed SST and radiative heat flux anomalies, Frankignoul and Kestenare (2002) show that SST-cloud radiative feedback is positive in most of the South Atlantic and negative near the equator, a result in support of ours.

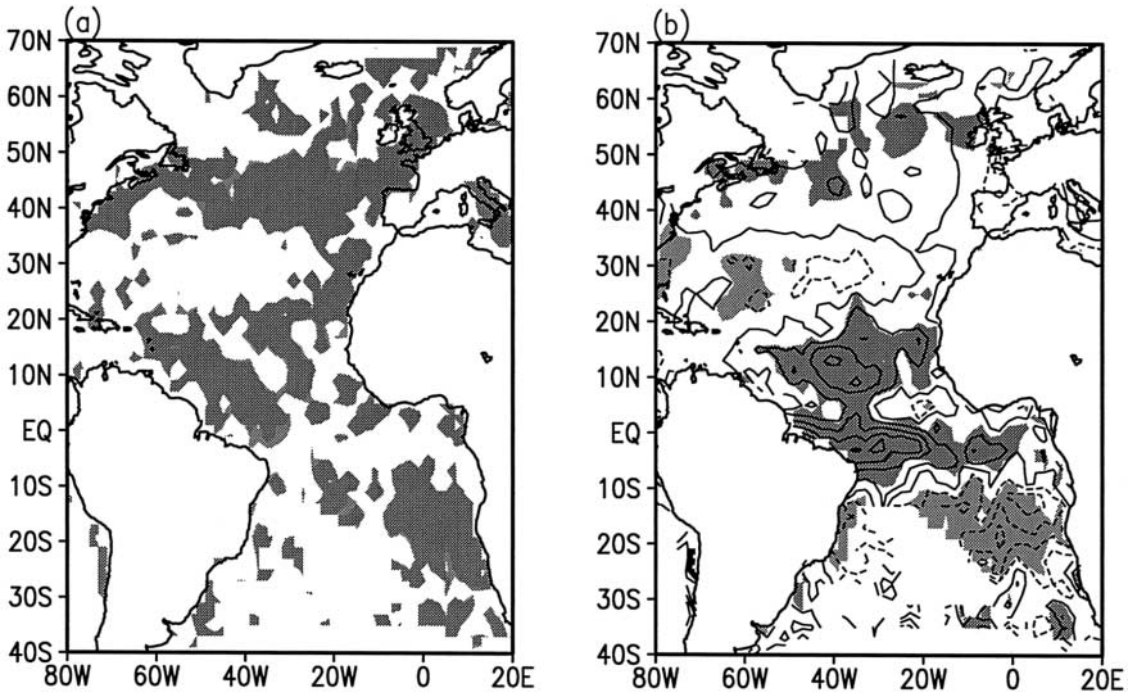

Fig. 13. (a) Ratio of low-level to total cloud cover anomalies in Fig. 10a. The regions with this ratio exceeding 90% are shaded. (b) The Feb.–Apr. downward total radiative flux anomalies at the sea surface (contours). Contour interval is 5 Wm^{-2}. The heavy (light) shading denotes shortwave heating (cooling) rate over 5 Wm^{-2}.

clouds in the Atlantic is captured to some extent in recent stand-alone (Okumura et al. 2001) and hybrid-coupled (Xie and Saito 2001) atmospheric GCM simulations.

This SST-stratus feedback is important for keeping the climatological ITCZ north of the equator in the Pacific (Philander et al. 1996). Here we show that it also operates on decadal time scales in the off-equatorial tropical and subtropical Atlantic. In a coupled ocean-atmosphere model, the temporal spectrum of the dipole mode response to white-noise forcing is sensitive to the damping rate in the SST equation (Xie and Tanimoto 1998; Xie 1999). The SST dependence of surface evaporation is a major mechanism for thermal damping, which can be linearized as a Newtonian cooling term with an e-folding time of 1 year (Xie 1999). The rate of SST change due to radiative forcing by low-level clouds is $-0.62(1-A)S_0C'/(c_p\rho H)$, where we have used Reed's (1977) formula for shortwave radiation, $S_0 = 300$ Wm^{-2} is the solar radiation in clear sky, $A = 0.96$ the albebo of sea surface, C' the perturbation cloud amount, c_p and ρ are the specific heat at constant pressure and density of sea water, and $H = 50$ m is the mixed layer depth. Assuming that low-level clouds in off-equatorial tropics vary with local SSTs, we have $C' = -\alpha T'$ with $\alpha = 0.1$ K^{-1} from the right panels of Fig. 10. This leads to an SST-stratus feedback coefficient, $b = 0.62\alpha(1-A)S_0/(c_p\rho H) = (3.5 \text{ years})^{-1}$. Thus the local SST-stratus feedback can reduce the Newtonian cooling rate for SST by as much as 30%.

Decadal SST variance in boreal winter features a local maximum on either side of the equator (Fig. 11a). Yet zonal wind variance is much smaller in the southern than northern subtropics. This latitudinal asymmetry of zonal wind variance is also present on interannual time scales in both the ship-board and satellite datasets (Fig. 11b). By contrast, the cloud anomaly pattern in the South Atlantic is robust and present in all seasons (Fig. 14). On both the annual and boreal-winter means, the cloudiness anomalies in the southern subtropics are about twice as large as the northern ones. Such

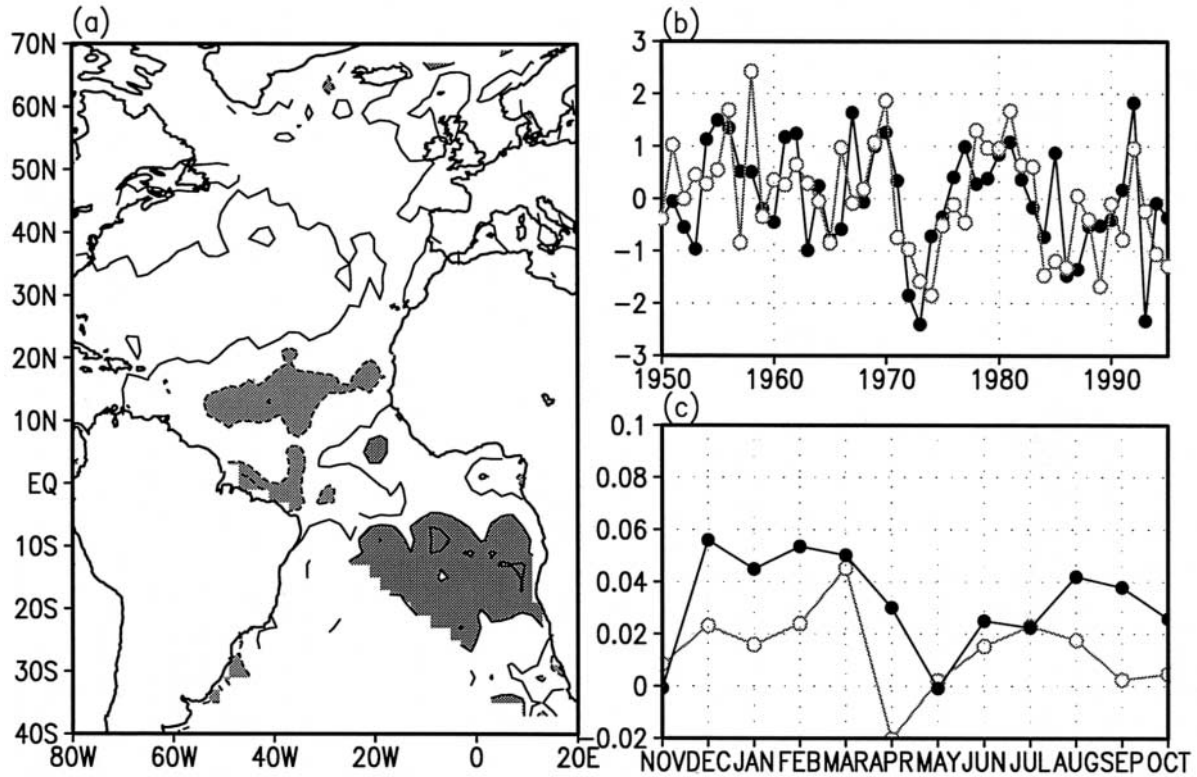

Fig. 14. (a) Annual-mean PADO composite for total cloud cover (contour at intervals of 3.0%, with light shade $<-3.0\%$ and heavy shade $>3.0\%$). (b) Normalized interhemispheric differences between the northern and southern tropics of cloud cover (solid circles) and SST (open circles). Here, unfiltered annual-mean anomalies are averaged zonally from coast to coast and meridionally in the 15–25° (10–20°) band for cloud (SST). (c) Decadal cloudiness anomalies averaged in 15–25° over the South (solid) and North (open circles) Atlantic, as a function of calendar month. The sign of the North Atlantic anomalies is reversed.

stronger stratus feedback can help the tropical South Atlantic maintain a level of SST variability comparable to the North Atlantic. We caution, however, that the true level of wind variability in the South Atlantic remains to be determined from longer satellite observations as has been discussed in Section 4.2.

6. Discussion: Origin of PADO

The poleward displacement of the SLP center from the tropical SST center in the North Atlantic—and to a lesser degree, in the South Atlantic—is quite peculiar and inexplicable with baroclinic models linearized about a resting state; such models predict SLP and SSTA centers more or less coinciding with each other (Matsuno 1966; Gill 1980; Lindzen and Nigam 1987). Such discrepancies between linear baroclinic models and observed surface wind variability in the tropical Atlantic are independently noted by Okumura et al. (2001), Seager et al. (2001) and Chung et al. (2002). A comparison of the composite height anomalies at 1000 and 500 hPa (Fig. 15) explains this deficiency of baroclinic models; Most of the SLP anomalies are the surface signature of a barotropic stationary seesaw between the subtropical and high-latitude North Atlantic. Because the barotropic height anomaly center at 35°N induces surface wind anomalies that extend well into the tropics, atmospheric models for the tropical Atlantic will need to include this barotropic mode and its interaction with baroclinic modes and the mean flow.

From observations alone, it is difficult to determine the origin of the NAO-like barotropic seesaw in the extratropical North Atlantic. Based on a single realization of atmospheric

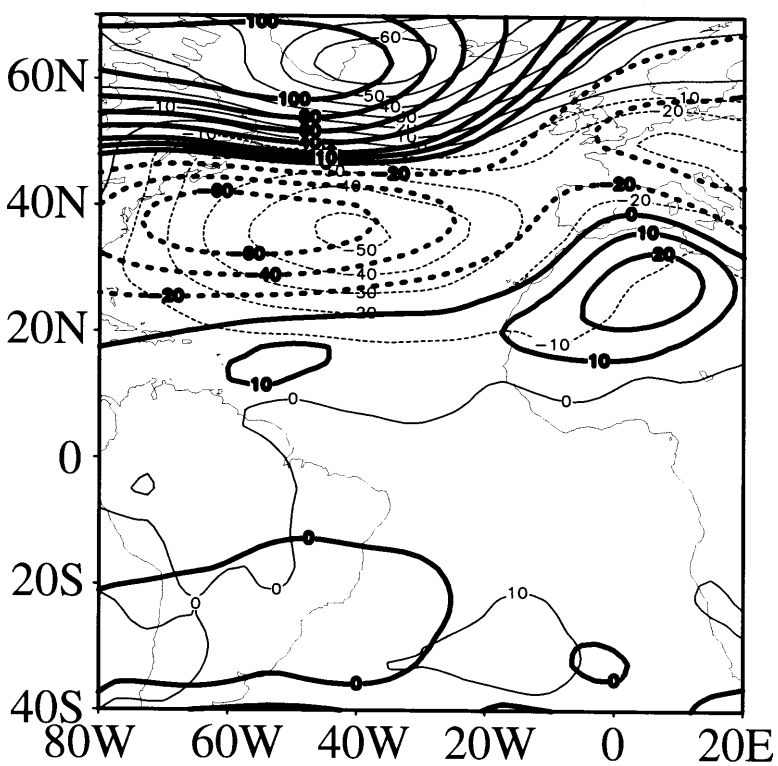

Fig. 15. Same as Fig. 7, but for geopotential height at 1000 hPa (thin contours) and 500 hPa (thick) from the NCEP reanalysis.

GCM simulation forced by observed SST history, Robertson et al. (2000) and Watanabe and Kimoto (1999) suggest that the shift in the Atlantic ITCZ may induce a barotropic response with a strong projection on the NAO. Okumura et al. (2001) force an atmospheric GCM with a time-invariant SST dipole in the tropical Atlantic and make a long-time integration to suppress the internal chaotic variability of the extratropical atmosphere. They obtain a robust barotropic response in the subtropical North Atlantic much like the one in Fig. 15 with anomalously intense cold surges on the east coast of North America. Similar results are obtained by using the ensemble simulation technique (N.-C. Lau 2000 personal comm.; Sutton et al. 2001). Coupling their atmospheric GCM with a slab ocean mixed layer, Okumura et al. further show that the extratropical part of the North Atlantic SST tripole is partly forced by the tropical SST dipole through this barotropic atmospheric bridge.

These GCM results may imply a tropics-to-extratropics forcing, but extratropical SSTAs may also induce NAO-like response as suggested by Rodwell et al. (1999) and Mehta et al. (2000). Regardless of its origin, the NAO can induce changes in the trade winds and hence the SSTAs in the tropical North Atlantic. Xie and Tanimoto (1998) show that forced by the observed wind variability in the extratropics, a tropical coupled model can reproduce much of the observed cross-equatorial SST gradient variability, suggesting an extratropics-to-tropics forcing. In fact, the SLP signal associated the NAO propagates equatorward (Halliwell 1997) and then it could change the sign of trade wind anomaly. Thus, the tropical SST dipole, the ITCZ and the North Atlantic subtropical high are probably engaged in a two-way interaction between the tropics and extratropics. The interhemispheric PADO pattern in this and other studies is most likely a result of such an interaction.

7. Summary

We have examined the time-space structures of decadal variability in the Atlantic Ocean

using various observational datasets of marine meteorological variables. We performed two pairs of EOF analyses separately for the North and South Atlantic: one pair for SST and one for SLP variability. While these two pairs of sub-datasets form statistically independent samples, the PCs of their respective leading EOFs are significantly correlated. The same EOF analysis has been repeated using a longer record of SST observations for three different periods of the 20th century. The results suggest that an interhemispheric PADO pattern—which consists of a tripole in the North and a dipole in the South Atlantic—exists throughout the entire 20th century. The leading SST EOFs separately obtained for the North and South Atlantic form a meridional dipole across the equator, a SSTA configuration maximizing cross-equatorial SST gradient anomalies. Given the high sensitivity of the Atlantic ITCZ to cross-equatorial SST gradient, we suggest that the association of the tropical SST dipole with the PADO is not accidental but is the centerpiece that links climate variability over the whole Atlantic Ocean together. Our analysis here and recent GCM studies (Okumura et al. 2001; Sutton et al. 2001; N.-C. Lau 2000, personal comm.) corroborate the association between the ITCZ and barotropic variability in the subtropical North Atlantic. This barotropic anomaly center contributes significantly to surface wind variability in the tropical North Atlantic.

Wind-induced latent heat flux is the major forcing for the SST tripole in the North Atlantic, consistent with previous studies (Deser and Blackmon 1993; Seager et al. 2000; Okumura et al. 2001; Lau and Nath 2001), with sensible heat flux making significant contributions in the high-latitudes. In the South Atlantic, by contrast, COADS wind anomalies are not well organized spatially and do not even satisfy the geostrophic balance with SLP anomalies. Our comparison with satellite wind measurements indicates that this poor spatial organization of COADS wind variability in the South Atlantic is due to the lack of ship observations there. Assimilating SLP measurements, the NCEP reanalysis yields improved the wind anomaly pattern but its variance is still much weaker than in the North Atlantic. The characteristics of South Atlantic wind variability and its relation with SST are a subject of future investigations.

We have detected a spatially coherent cloud anomaly pattern in both the North and South Atlantic. In the off-equatorial tropics poleward of 10°, low-level cloud cover increases with decreasing SST, and its shielding of solar radiation leads to a positive feedback between the clouds and SST, which can reduce SST damping rate by as much as 30%. Compared to the tropical North Atlantic, this cloud-SST feedback appears to be twice as strong in the South Atlantic, helping maintain SST variability there despite weak variability in COADS wind.

Our analysis suggests an interhemispheric decadal mode that spans the whole Atlantic basin from the southern tip of South America to Greenland and appears to exist for the 20th century. Proxy-based climate records in the equatorial Atlantic also indicate an existence of this decadal mode prior to last century (Black et al. 1999; Cobb et al. 2001). By no means, however, this implies that it is the only or even the dominant mode of Atlantic climate variability. In fact, this PADO mode accounts for 4–5% total unfiltered variance (40% in the 8–16-year decadal band) over the whole Atlantic. Atlantic variability is affected by many factors; Pacific ENSO forcing (Enfield and Meyer 1997; Chang et al. 2000; Lau and Nath 2001), stochastic forcing by the NAO (Xie and Tanimoto 1998) and other atmospheric modes, the equatorial mode (Zebiak 1993; Carton et al. 1996) and slow ocean dynamics (Eden and Willebrand 2001) are just some examples that can give rise to variability other than the PADO mode. The present study offers a view from the perspective of separate EOF analysis for the North and South Atlantic. Empirical and modeling studies from other angles are necessary to advance our understanding of Atlantic variability. To achieve this goal, we call for enhanced observations of the South Atlantic, both in-situ and by using new satellite remote-sensing technology. Data archeology (e.g., Manabe 1999) and proxy-based paleoclimate reconstruction are also highly desired.

Acknowledgment

The authors are grateful to Profs. T. Yamagata, H. Nakamura, N. Iwasaka and T. Matsuno for stimulating discussions. We also thank

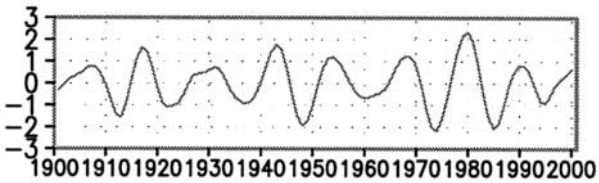

Fig. A1. Normalized principal component (PC) of SST anomalies in the entire Atlantic. This PC is calculated from performing EOF analysis for mostly updated GISST anomalies from 1901–2000.

the NOAA/NCEP for providing the reanalysis data and the NCAR for providing the COADS/LMRF dataset. This work is supported by the Frontier Research System for Global Change and NOAA CLIVAR Atlantic Program through grant NA17RJ1230. The IPRC contribution #164 and SOEST #6009.

Appendix

Figure A1 represents mostly updated PADO index from 1901 through 2000. This index is calculated from performing the EOF analysis for updated GISST over the entire Atlantic. The exact values over 100 years are available on 'http://wwwoa.ees.hokudai.ac.jp/people/tanimoto/'.

References

Alexander, M.A., 1992: Midlatitude atmosphere-ocean interaction during El Niño. Part I: The North Pacific Ocean. *J. Climate*, **5**, 944–958.

Black, D.E., L.C. Peterson, J.T. Overpeck, A. Kaplan, M.N. Evans and M. Kashgarian, 1999: Eight centuries of North Atlantic Ocean atmosphere variability. *Science*, **286**, 1709–1713.

Carton, J.A., X. Cao, B.S. Giese and A.M da Silva, 1996: Decadal and interannual SST variability in the tropical Atlantic Ocean. *J. Phys. Oceanogr.*, **26**, 1165–1175.

Cayan, D.R., 1992: Latent and sensible heat fluxes over the Northern oceans: the connection to monthly atmospheric circulation. *J. Climate*, **5**, 354–396.

Chang, P., L. Ji and H. Li, 1997: A decadal climate variation in the tropical Atlantic Ocean from thermodynamic air-sea interaction. *Nature*, **385**, 516–518.

———, R. Saravanan, L. Ji. and G.C. Hegerl, 2000: The effect of local sea surface temperatures on atmospheric circulation over the tropical Atlantic sector. *J. Climate*, **13**, 2195–2216.

———, L. Ji and R. Saravanan, 2001: A hybrid coupled model study of tropical Atlantic variability. *J. Climate*, **14**, 361–390.

Chiang, J.C.H., Y. Kushnir and S.E. Zebiak, 2000: Interdecadal changes in eastern Pacific ITCZ variability and its influence on the Atlantic ITCZ. *Geophys. Res. Lett.*, **27**, 3687–3690.

Chung, C., S. Nigam and J.A. Carton, 2002: SST-forced surface wind variability in the tropical Atlantic: An empirical model. *J. Geophys. Res.-Atmos.*, submitted.

Clark, N.E., L. Eber, R. Laurs, J. Renner and J. Saur, 1974: Heat exchange between ocean and atmosphere in the eastern North Pacific for 1961–71, *NOAA Tech. Rep.* NMFS SSRF-682.

Cobb, K.M., C.D. Charles and D.E. Hunter, 2001: A central tropical Pacific coral demonstrates Pacific, Indian and Atlantic decadal climate connections. *Geophys. Res. Lett.*, **28**, 2209–2212.

Deser, C. and M.L. Blackmon, 1993: Surface climate variations over the North Atlantic Ocean during winter: 1900–1989. *J. Climate*, **6**, 1743–1753.

Dommenget, D. and M. Latif, 2000: Interannual to decadal variability in the tropical Atlantic. *J. Climate*, **13**, 777–792.

Eden, C. and J. Willebrand, 2001: Mechanism of interannual to decadal variability of the North Atlantic circulation. *J. Climate*, **14**, 2266–2280.

Enfield, D.B. and D.A. Mayer, 1997: Tropical Atlantic sea surface temperature variability and its relation to El Niño-Southern Oscillation. *J. Geophys. Res.*, **102**, 929–945.

———, A.M. Mestas-Nuñez, D.A. Mayer and L. Cid-Serrano, 1999: How ubiquitous is the dipole relationship in tropical Atlantic sea surface temperatures? *J. Geophys. Res.*, **104**, 7841–7848.

Folland, C.K. and D.E. Parker, 1995: Correction of instrumental biases in historical sea surface temperature data, *Quart. J. Roy. Meteor. Soc.*, **121**, 319–367.

Frankignoul, C. and E. Kestenare, 2002: The surface heat flux feedback. Part I: estimates from observation in the Atlantic and the North Pacific. *Clim. Dyn.*, submitted.

Gill, A.E., 1980: Some simple solutions for heat-induced tropical circulation. *Quart. J. Roy. Meteor. Soc.*, **106**, 447–462.

Häkkinen, S. and K.C. Mo, 2002: The low-frequency variability of the tropical Atlantic Ocean. *J. Climate*, **15**, 237–250.

Halliwell, G.R., 1997: Decadal and multidecadal

North Atlantic SST anomalies driven by standing and propagating basin-scale atmospheric anomalies. *J. Climate*, **10**, 2405–2411.

——— and D.A. Mayer, 1996: Frequency response properties of forced climatic SST anomaly variability in the North Atlantic. *J. Climate*, **9**, 3575–3587.

Hashizume, H., S.-P. Xie, W.T. Liu and K. Takeuchi, 2001: Local and remote atmospheric response to tropical instability waves: A global view from the space. *J. Geophys. Res.-Atmos.*, **106**, 10173–10185.

Hastenrath, S. and L. Heller, 1977: Dynamics of climate hazards in northeast Brazil. *Quart. J. Roy. Meteor. Soc.*, **103**, 77–92.

Houghton, R.W. and Y.M. Tourre, 1992: Characteristics of low-frequency sea surface temperature fluctuations in the tropical Atlantic. *J. Climate*, **5**, 765–771.

Huang, B., J.A. Carton and J. Shukla, 1995: A numerical simulation of the variability in the tropical Atlantic ocean, 1980–88. *J. Phys. Oceanogr.*, **25**, 835–854.

——— and J. Shukla, 1997: Characteristics of the interannual and decadal variability in a general circulation model of the tropical Atlantic Ocean. *J. Phys. Oceanogr.*, **27**, 1693–1712.

Iwasaka, N. and K. Hanawa, 1990: Climatologies of marine meteorological variables and surface fluxes in the North Pacific computed from COADS. *Tohoku Geophys. J.*, **33**, 185–239.

Jones, P.D., T.J. Osborn, K.R. Briffa, C.K. Folland, E.B. Horton, L.V. Alexander, D.E. Parker and N.A. Rayner, 2001: Adjusting for sampling density in grid box land and ocean surface temperature time series. *J. Geophys. Res.*, **106**, 3371–3380.

Kalnay, E., M. Kanamitsu, R. Kistler, W. Collins, D. Deaven, L. Gandin, M. Iredell, S. Saha, G. White, J. Woolen, Y. Zhu, M. Chelliah, W. Ebisuzaki, W. Higgins, J. Janowiak, K.C. Mo, C. Ropelewski, J. Wang, A. Leetmaa, R. Reynolds, R. Jenne and D. Joseph, 1996: The NCEP/NCAR 40-year reanalysis project. *Bull. Amer. Meteor. Soc.*, **77**, 437–471.

Klein, S.A. and D.L. Hartmann, 1993: The seasonal cycle of low stratiform clouds, *J. Climate*, **6**, 1587–1606.

Kondo, J., 1975: Air-sea bulk transfer coefficient in diabatic conditions. *Bound-Layer Meteor*, **9**, 91–112.

Kushnir, Y., 1994: Interdecadal variation in North Atlantic sea surface temperature and associated atmospheric circulation. *J. Climate*, **7**, 141–157.

Lamb, P.J., 1978: Large-scale tropical Atlantic surface circulation patterns associated with Subsaharan weather anomalies. *Tellus*, **30**, 240–251.

Lau, N.-C. and M.J. Nath, 1996: The role of the "atmospheric bridge" in linking tropical Pacific ENSO events to extratropical SST anomalies. *J. Climate*, **9**, 2036–2057.

——— and ———, 2001: Impact of ENSO on SST variability in the North Pacific and North Atlantic: Seasonal dependence and role of extratropical air-sea coupling. *J. Climate*, **14**, 2846–2866.

Lindzen, R.S. and S. Nigam, 1987: On the role of sea surface temperature gradients in forcing low level winds and convergence in the tropics. *J. Atmos. Sci.*, **44**, 2418–2436.

Manabe, T., 1999: The digitized Kobe Collection, Phase I: historical surface marine meteorological observations in the archive of the Japan Meteorological Agency. *Bull. Amer. Meteor. Soc.*, **80**, 2703–2715.

Matusno, T., 1966: Quasi-geostrophic motions in the equatorial area. *J. Meteor. Soc. Japan*, **44**, 25–43.

Mehta, V.M., 1998: Variability of the tropical ocean surface temperatures at decadal-multidecadal timescales. Part I: the Atlantic Ocean. *J. Climate*, **11**, 2351–2375.

——— and T. Delworth, 1995: Decadal variability of the tropical Atlantic Ocean surface temperature in shipboard measurements and in a global ocean-atmosphere model. *J. Climate*, **8**, 172–190.

———, M.J. Suarez, J. Manganello, and T.L. Delworth, 2000: Oceanic influence on the North Atlantic oscillation and associated northern hemisphere climate variations. *Geophys. Res. Lett.*, **27**, 121–124.

Mestas-Nuñez, A.M. and D.B. Enfield, 1999: Rotated global modes of non-ENSO sea surface temperature variability. *J. Climate*, **12**, 2734–2746.

Nobre, P. and J. Shukla, 1996: Variations of sea surface temperature, wind stress, and rainfall over the tropical Atlantic and South America. *J. Climate*, **9**, 2464–2479.

Okumura, Y., S.-P. Xie, A. Numaguti and Y. Tanimoto, 2001: Tropical Atlantic air-sea interaction and its influence on the NAO. *Geophys. Res. Lett.*, **28**, 1507–1510.

Park, S. and C.B. Leovy, 2000: Winter North Atlantic low cloud anomalies associated with the Northern Hemisphere annular mode. *Geophys. Res. Lett.*, **20**, 3357–3360.

Parker, D.E., P.D. Jones, A. Bevan and C.K. Folland, 1994: Interdecadal changes of surface temperature since the late 19th century. *J. Geophys. Res.*, **99**, 14373–14399.

———, C.K. Folland and M. Jackson, 1995: Marine surface temperature: observed variations and data requirements. *Clim. Change*, **31**, 559–600.

Philander, S.G.H., D. Gu, D. Halpern, G. Lambert, N.-C. Lau, T. Li and R.C. Pacanowski, 1996: The role of low-level stratus clouds in keeping the ITCZ mostly north of the equator. *J. Climate*, **9**, 2958–2972.

Rajagopalan, B., Y. Kushnir and Y.M. Tourre, 1998: Observed decadal midlatitude and tropical Atlantic climate variability. *Geophys. Res. Lett.*, **25**, 3967–3970.

Reed, R.K., 1977: On estimating insolation over the ocean. *J. Phys. Oceanogr.*, **7**, 482–485.

Robertson, A.W., C.R. Mechoso and Y.-J. Kim, 2000: The influence of Atlantic sea surface temperature anomalies on the North Atlantic Oscillation. *J. Climate*, **13**, 122–138.

Rodwell, M.J., D.P. Rowell and C.K. Folland, 1999: Oceanic forcing of the wintertime North Atlantic oscillation and European climate. *Nature*, **398**, 320–323.

Ruiz-Barradas, A., J.A. Carton and S. Nigam, 2000: Structure of interannual-to-decadal climate variability in the tropical Atlantic sector. *J. Climate*, **13**, 3285–3297.

Seager, R., Y. Kushnir, M. Visbeck, N. Naik, J. Miller, G. Krahmann and H. Cullen, 2000: Causes of Atlantic Ocean climate variability between 1958–1998. *J. Climate*, **13**, 2845–2862.

———, ———, P. Chang, N. Naik, J. Miller and W. Hazeleger, 2001: Looking for the role of the ocean in tropical Atlantic decadal climate variability. *J. Climate*, **14**, 638–655.

Servain, J., 1991: Simple climatic indices for the tropical Atlantic Ocean and some applications. *J. Geophys. Res.*, **96**, 15137–15146.

Sutton, R.T., W.A. Norton and S.P. Jewson, 2001: The North Atlantic Oscillation—What role for the ocean? *Atmos. Sci. Lett.*, **1**, 89–100.

Tanimoto, Y., N. Iwasaka and K. Hanawa, 1997: Relationship between sea surface temperature, the atmospheric circulation and air-sea fluxes on multiple time scales. *J. Meteor. Soc. Japan*, **75**, 831–849.

——— and S.-P. Xie, 1999: Ocean-Atmosphere Variability over the Pan-Atlantic basin. *J. Meteor. Soc. Japan*, **77**, 31–46.

Tomita, T., S.-P. Xie and M. Nonaka, 2002: Relationship between decadal surface and subsurface variability in the midlatitude North Pacific. *J. Climate*, submitted.

Tourre, Y.M., B. Rajagopalan and Y. Kushnir, 1999: Dominant Patterns of Climate Variability in the Atlantic Ocean during the Last 136 Years. *J. Climate*, **12**, 2285–2299.

Venegas, S.A., L.A. Mysak and D.N. Straub, 1997: Atmosphere-ocean coupled variability in the South Atlantic. *J. Climate*, **10**, 2904–2920.

Wagner, R.G., 1996: Mechanisms controlling variability of the interhemispheric sea surface temperature gradient in the tropical Atlantic. *J. Climate*, **9**, 2010–2019.

Watanabe, M. and M. Kimoto, 1999: Tropical-extratropical connection in the Atlantic atmosphere-ocean variability. *Geophys. Res. Lett.*, **26**, 2247–2250.

———, ———, T. Nitta and M. Kachi, 1999: A comparison of decadal climate oscillations in the North Atlantic detected in observations and a coupled GCM. *J. Climate*, **12**, 2920–2940.

Woodruff, S.D., R.J. Slutz, R.L. Jenne and P.M. Steurer, 1987: A comprehensive ocean-atmosphere dataset. *Bull. Amer. Meteor. Soc.*, **68**, 521–527.

Xie, S.-P., 1999: A dynamic ocean-atmosphere model of the tropical Atlantic decadal variability. *J. Climate*, **12**, 64–70.

——— and S.G.H. Philander, 1994: A coupled ocean-atmosphere model of relevance to the ITCZ in the eastern Pacific. *Tellus*, **46A**, 340–350.

——— and K. Saito, 2001: Formation and variability of a northerly ITCZ in a hybrid coupled AGCM: Continental forcing and ocean-atmospheric feedback. *J. Climate*, **14**, 1262–1276.

——— and Y. Tanimoto, 1998: A Pan-Atlantic decadal climate oscillation. *Geophys. Res. Lett.*, **25**, 2185–2188.

———, ———, H. Noguchi and T. Matsuno, 1999: How and why climate variability differs between the tropical Atlantic and Pacific. *Geophys. Res. Lett.*, **26**, 1609–1612.

Zebiak, S., 1993: Air-sea interaction in the equatorial Atlantic region. *J. Climate*, **6**, 1567–1586.